I&EC research
Industrial & Engineering Chemistry Research

pubs.acs.org/IECR
Article

Mass Transfer of CO_2 in Amine-Functionalized Structured Contactors in Ultra-Dilute Conditions

Quirin Grossmann and Marco Mazzotti*

Cite This: *Ind. Eng. Chem. Res.* 2025, 64, 2339−2353
Read Online

ACCESS | Metrics & More | Article Recommendations | Supporting Information

ABSTRACT: Extracting CO_2 from the atmosphere via direct air capture (DAC) provides a pathway to counteract the rising CO_2 concentration in the atmosphere. Processes using amine functionalized solid sorbents have attracted considerable attention, as they exhibit high affinity toward CO_2 at atmospheric concentrations. The process is significantly influenced by the mass transfer kinetics of adsorption, and accurate quantification is crucial for improving process models and DAC systems. In this study, we addressed this critical issue by quantifying the mass transfer kinetics of three amine functionalized structured sorbents: two alumina pellets with unimodal (TRI@unimodal) and bimodal (TRI@bimodal) pore size distributions, and a honeycomb mullite/alumina monolith (TRI@monolith). A modeling framework was developed to enable the use of a commercial volumetric sorption device to measure sorbent mass transfer kinetics, and to distinguish them from resistances within the device. The measurements revealed distinct mass transfer regimes, with pore diffusion playing a significant role in the bimodal pellets, whereas a surface resistance introduced by the functionalization procedure dominated in the unimodal pellets. The device was unable to capture the pore diffusion in the monolith due to instrument resistances limiting this regime. A self-limiting diffusion behavior previously reported in literature was identified in the amine layer, which decreased diffusion with increasing CO_2 uptake. We estimate kinetic parameters for all three sorbent materials for use in a widely used linear driving force (LDF) model adapted for amine functionalized sorbents. The parameter describing the mass transfer in the gas phase is nearly five times larger for TRI@bimodal than for TRI@unimodal. For the mass transfer in the amine layer, the parameter increases progressively from TRI@monolith to TRI@unimodal to TRI@bimodal. The results highlight the importance of pore structure and functionalization procedure to improve DAC sorbents.

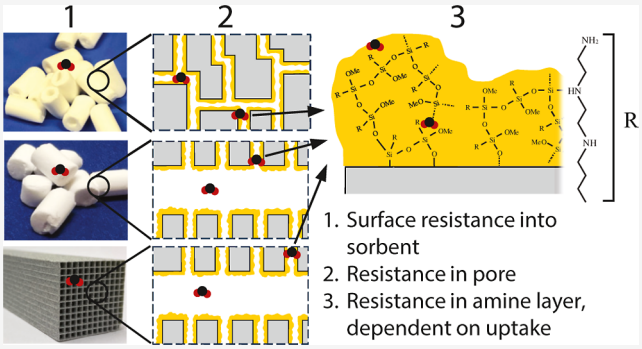

INTRODUCTION

Direct air capture (DAC) is establishing itself as a viable method of extracting CO_2 from the atmosphere and, when combined with suitable storage techniques, can be considered a carbon dioxide removal (CDR) technology.[1−3] A proven method to achieve the extraction is to flow ambient air through a structure containing solid sorbents that have a high affinity to CO_2 at atmospheric conditions.[4,5] The sorbents can then be regenerated, and the CO_2 collected, using a temperature-vacuum swing adsorption (TVSA) cycle.[6,7] Significant effort is currently being put into making this and other DAC processes more economical and energy efficient to increase their attractiveness as a CDR solution. These efforts include sorbent development and characterization,[8] together with modeling and optimization of the process.[6,7,9] A critical aspect in the modeling of a DAC process is the ability to describe the transport of CO_2 within solid sorbents.[6,9,10] The rate of this transport has been found to have a large impact on the productivity of the DAC process, and therefore on its estimated cost and energy demand.[9,11] This is especially true for the adsorption step, which can be as much as five times longer than the regeneration step.[5,12] Accurate modeling of the adsorption kinetics is therefore crucial to enable both the accurate modeling of the process and the further development of sorbent materials. The task is made more complex by the variability of feed conditions experienced in the DAC process as well as by the novel materials used. This is reflected in the limited availability of kinetic data in open literature, especially when compared to the large amount of works describing novel materials for DAC.

One of the most common sorbent materials used for DAC is amine-functionalized metal oxides.[13] The advantages of these materials are well-known, and include the strong affinity to CO_2 under ultradilute conditions and the resistance to

Received: October 28, 2024
Revised: December 13, 2024
Accepted: December 18, 2024
Published: January 13, 2025

https://doi.org/10.1021/acs.iecr.4c04099
Ind. Eng. Chem. Res. 2025, 64, 2339−2353

humidity.[14] The limiting mass transfer mechanisms of these materials are less explored, especially for structured sorbents. While some works qualitatively address the kinetics using metrics such as adsorption half-time,[15,16] few quantify them well enough that they can be used in process models. In structured amine-functionalized sorbents, at least three mass transfer resistances can be identified:

- External resistances as a result of the structure, such as film and bed resistances;
- Resistances within the pores, such as the mesopores of a porous sorbent;
- Resistances in the amine layer of the sorbent.

For structured sorbents such as pellets or honeycomb monoliths, well-known correlations for external mass transfer resistances can be used.[5,17] Further established correlations exist to describe the diffusion within the pores of the pellets and of the monolith walls, such as Knudsen or molecular diffusion.[18−20] For amine-functionalized sorbents, further resistances can arise due to the functionalization.[21] Studies on the kinetics of such materials have often found two distinct regimes of mass transfer. The fast regime is generally assumed to be pore diffusion controlled, while several mechanisms have been postulated to be responsible for the slow mass transfer regime. They can be loosely grouped as follows:

1. Diffusional resistance in the amine layer to less accessible adsorption sites in the bulk of the layer[21−23]
2. Reaction kinetics between the CO_2 molecules and the amines[24−30]
3. A combination of both the mechanisms above[31−34]

The first approach claims that the functionalization procedure introduces a layer of polymerized amines, creating heterogeneous adsorption sites with differing accessibility.[21] The easily accessible sites are assumed to be on the surface of the amine layer, while the sites in the bulk are assumed to be less accessible and therefore subject to additional mass transfer resistance. The second approach claims that the reaction kinetics between the CO_2 and the amines is the limiting mechanism in the slow mass transfer regime.[24−30] The third approach combines the first two mechanisms, with some models including diffusion to the vicinity of the amine sites, followed by chemical reaction.[33] By modeling experiments to include both effects, it was found that the characteristic time of diffusion in the support layer is significantly larger than that of reaction at low relative humidity.[33] However, the nature of the slow diffusion mechanism can depend on sorbent characteristics such as the loading of functional groups. High loadings lead to increased diffusional resistances,[32,34] while at low loadings the reaction rate can become controlling.[34] Recently, Vallace et al.[32] described a self-inhibiting diffusion mechanism as a direct consequence of the chemical reaction between the CO_2 and the amine functionalities, which can create cross-linking between the amines and thereby inhibit diffusion, while the reaction rate only influences the initial part of the adsorption. In this work, we use the diffusion approach to model the slow mass transfer regime, as those studies that included both reaction rate and diffusion mechanisms found that the diffusion mechanism is likely rate-limiting for most of the uptake.[32,33]

Performing measurements to extract accurate kinetic parameters requires care to avoid misinterpretation of the results, regardless of the measurement technique. All experimental phenomena should be included in the model that is used to fit the data in order to extract accurate kinetic data.[35] Many of the above-mentioned kinetic measurements were performed using dynamic column breakthrough techniques. While this measurement technique arguably best represents the conditions in which sorbents are used, it often includes many different phenomena, such as axial dispersion and bed effects.[36] Separating all these effects can be challenging and possibly lead to less accurate estimation of model parameters. Batch measurements such as gravimetric and volumetric measurements are alternative techniques that, if designed correctly, can reduce the number of phenomena affecting the measurement.[19,35,37,38] The devices required for such measurements are often available in laboratories that study adsorption as they are used to determine equilibrium isotherms. A significant difference in volumetric measurements compared to the other measurement techniques is that the partial pressure of CO_2 is typically regulated by adjusting the absolute pressure using pure CO_2, rather than mixing CO_2 with an inert carrier gas to reach the intended concentration. Furthermore, the pressure changes significantly within the adsorption chamber during a measurement step due to the CO_2 being adsorbed, which must be taken into account for the modeling.[20,39]

This work aims to contribute to the lack of kinetic information on CO_2 on amine-functionalized metal oxides in open literature by using a commercial volumetric device to quantify adsorption under dry conditions on three triamine grafted alumina adsorbents with differing pore structures. This is achieved by providing (1) new models and kinetic parameters for the studied materials, while also (2) a framework for using widely used commercial volumetric instruments to measure the kinetics in such materials. The results are put into context by showing their applicability in simplified kinetic correlations typically used in column models.

MATERIALS

Anhydrous toluene (99.8%) and 3-[2-(2-aminoethylamino)-ethylamino]-propyltrimethoxysilane (TRI or triamine) were purchased from Sigma-Aldrich and stored under Argon atmosphere once opened. Extruded cylindrical alumina pellets SA6578 and SA6176 were kindly contributed by Saint Gobain (France). The diameter of both pellets was ca. 3 mm and the length was typically between 3 and 3.5 mm. The alumina washcoat precursor (Pural TH 200) was provided by Sasol (Germany) and applied to the mullite monoliths by HUG Engineering (Switzerland), which consisted of ca. 10 wt % washcoat; the size of the monoliths was 30 × 30 × 130 mm, with a CPSI of 100, channel size of 2 × 2 mm and a wall thickness of ca. 0.4 mm. After functionalization, 2 × 2 mm pieces were cut from the monolith for adsorption rate measurements. All gases were supplied by Linde with a purity of at least 4.5.

Functionalization. The functionalization procedure for both pellets and monoliths has been described in detail elsewhere.[40] In short, a wet grafting procedure was used to introduce the triamine onto the alumina surface of all the support materials. Prior to functionalization, the supports were dried at 120 °C for 16 h.

Pellets. The pellets were then added directly to anhydrous toluene, after which 75 μL of water was added per gram of support and stirred for 1 h. The temperature was then raised to 85 °C, a specific amount of triamine was added dropwise to the solution (930 μL $g^{-1}_{alumina}$ for SA6578 and 1000 μL $g^{-1}_{alumina}$ for

https://doi.org/10.1021/acs.iecr.4c04099
Ind. Eng. Chem. Res. 2025, 64, 2339−2353

SA6176 pellets) and the mixture was left to equilibrate for 12 h. The functionalized SA6578 pellets are referred to as TRI@unimodal, and the functionalized SA6176 pellets are referred to as TRI@bimodal from hereon based on the nature of the respective pore size distributions.

Monolith. The monolith was then hydrated by placing it in a water bath for 2 h at ca. 60 °C, after which it was dried to a mass that corresponds to 1.8 monolayers of water on the alumina surface. A solution of 500 mL anhydrous toluene and 16.5 mL triamine was prepared in a 500 mL thermostated reactor. This was stirred and heated to 85 °C, after which the hydrated monolith was added and allowed to equilibrate for 12 h.

Subsequently, all contactors were allowed to cool to room temperature, washed with toluene, ethanol, and diethyl ether, then allowed to dry for at least 24 h.

Material Characterization. N_2 sorption isotherms were measured on a Microtrac Belsorp Max at 77 K. Prior to each measurement, the samples were dried under vacuum at 100 °C for 3 h. The Brunauer−Emmet−Teller (BET) surface area was estimated using isotherm data in the relative pressure range of 0.05−0.25. The pore sizes were estimated using the Barrett−Joyner−Halenda (BJH) method on the desorption branch of the N_2 isotherms.[41]

The amount of nitrogen on the functionalized pellets was measured using elemental analysis for the pellets. The measurements were performed on a LECO TruSpec Micro instrument by the Molecular and Biomolecular Analysis Service (MoBiAS) at ETH Zurich. Due to the low amount of nitrogen on the monolith, elemental analysis did not provide reliable data. Therefore, the amount was estimated using the mass increase caused by functionalization.

XRD measurements were performed on powdered samples using a Bruker D2 Phaser second generation. For the monolith, a separate sample of wash-coat was measured to avoid overlapping signals with the mullite support.

Mercury intrusion measurements were performed by 3P-Instruments on a Quantachrome Poremaster 60-GT. Prior to the measurements, the samples were dried for 2 h at 100 °C in a furnace.

A detailed description of the piezometric mass transfer measurements is provided in the next section. Care was taken to use sorbent pieces of similar size for all measurements to avoid different length scales in the same measurement. Prior to each measurement, the sorbent was regenerated at 100 °C for 3 h under high vacuum. A leak check was performed to ensure the vials were properly sealed.

Adsorption Kinetics Measurements. The measurements to elucidate the mass transfer behavior of the adsorbents were performed using the piezometric method on a Microtrac Belsorp Max device. Piezometric measurements, commonly also referred to as volumetric measurements, involve tracking the pressure response to the addition or removal of sorbate in a closed vessel of constant, known volume containing the adsorbent.[19] The procedure is explained in more detail later. In principle, the pressure response is solely a function of the mass transfer kinetics in the sorbent and can be modeled using standard mass transfer models to determine kinetic coefficients.

In practice, several other effects influence the pressure response, including sorbent effects, such as heat transfer,[35] and instrument effects, such as mass transfer resistances within the instrument.[24,37,38,42] To avoid erroneous results, their impact should be minimized by using an appropriately designed experimental procedure, and it should be accounted for in the mass transfer model.[35] This section gives a detailed overview of the device, of the design of the experimental procedure, and of the sorption models used to accurately describe the mass transfer behavior.

Device. The device used in this work is shown in Figure 1 and, similarly to all conventional piezometric devices, consists

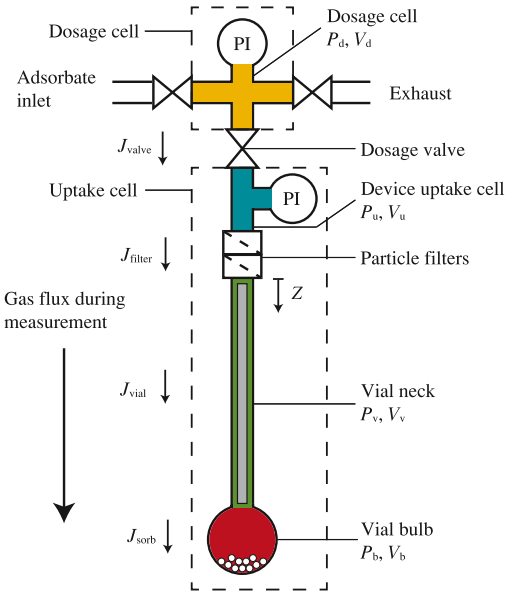

Figure 1. Schematic of the volumetric measurement device Belsorp Max including the definitions of the various volumes and flows that are modeled in eqs 19−22.

of a dosage cell and of an uptake cell separated by the dosage valve (see dashed lines). Here, the pressure can be monitored both in the dosage cell and the uptake cell. The latter is useful for equilibrium measurements where multiple samples are all connected to the same dosage cell, while the former is always used for kinetic measurements.

In the device used here, the uptake cell is divided into two parts: the device part (blue) and the vial (green and red) containing the sorbent, which are separated by particle filters to prevent contamination of the device. The vial holds the sorbent in a bulb (red) at the end of a long neck (green), which enables the immersion of the sorbent into an external thermal bath.

Typical Measurement Sequence. The measurements were performed using a typical approach for piezometric adsorption measurements,[38] which consists of the following steps:

1. The starting point is the equilibrium state of the previous step, so pressure $P_{u,0}$ for both dosage cell and uptake cell, and uptake q_0 for the sorbent. For the first measurement step, $P_{u,0} = 0$ and $q_0 = 0$.
2. The dosage valve is closed and the dosage cell is pressurized to $P_{d,0}$ through the adsorbate inlet, which is closed again once the desired pressure is reached.
3. The dosage valve is opened and the pressure in both cells equilibrates at P_0. The equilibration requires some time, while the gas from the dosage cell flows through the device components shown in Figure 1 before reaching the adsorbent.

https://doi.org/10.1021/acs.iecr.4c04099
Ind. Eng. Chem. Res. 2025, 64, 2339−2353

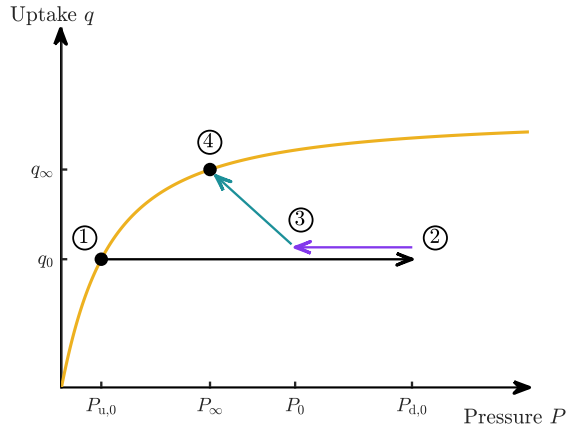

(a) A typical measurement step shown on the isotherm.

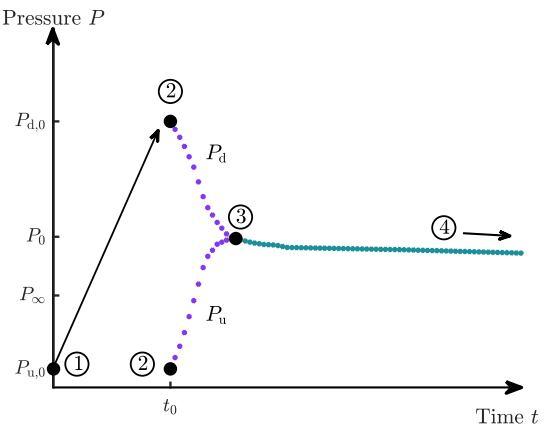

(b) The pressure profiles of both P_d and P_u of a typical measurement step.

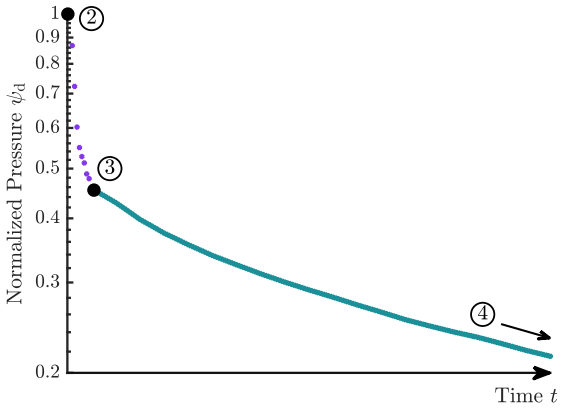

(c) The normalized pressure profile as given in Equation 1.

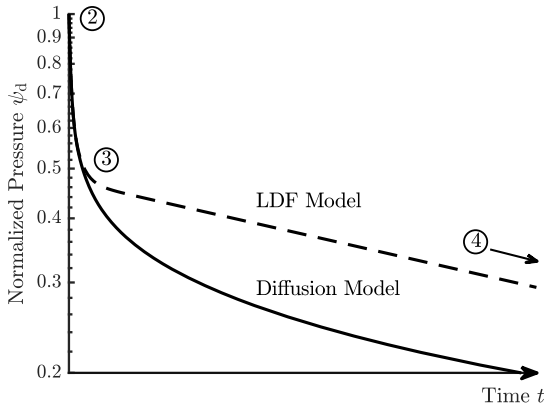

(d) Two modeling approaches to describe the mass transfer in the adsorbent.

Figure 2. Depiction of a typical measurement step in a measurement series. Multiple measurement steps are performed until the desired P_∞ is reached. Point 1 is the equilibrium state at the end of the previous measurement. Point 2 shows the dosage cell pressurization. Point 3 corresponds to the equilibration between dosage and uptake cell. The pressure profile between points 3 and 4 contains the information on sorption kinetics, assuming no other limitations.

4. The pressure continues to decrease due to adsorption until a predefined equilibrium condition is reached at P_∞, with the corresponding q_∞ in the adsorbent.

The steps are shown in Figure 2 in several different representations. In Figure 2a we use the equilibrium isotherm to show both the initial state (1) and the equilibrium state (4) of the measurement step, and how they are reached. The part of interest in each step to determine mass transfer kinetics is the phase after equilibration of the uptake and dosage cell, hence between point 3 and point 4. Note that the time taken for pressurization (1 → 2) and equilibration (2 → 3) is typically in the order of seconds, while the time of the adsorption step is typically in the order of minutes to hours depending on the kinetics of adsorption. The corresponding pressure profile is shown in Figure 2b, where the equilibration step of the dosage and uptake cell can be easily observed, followed by the adsorption step. In this representation, it is difficult to draw any qualitative conclusions about the mechanism that controls the adsorption behavior of the adsorbent. To enable a better analysis of this, a normalized pressure can be used and shown in a semilogarithmic plot (see Figure 2c).[19,35,38] The normalized pressure used in this work is defined as

$$\psi_d = \frac{P_d - P_\infty}{P_{d,0} - P_\infty} \tag{1}$$

where P_d is the pressure in the dosage cell and the subscript 0 denotes the pressure before opening the dosage valve (point 2); P_∞ is the equilibrium pressure reached at the end of the measurement step (point 4). In this representation, it can be distinguished which kinetic model best describes the mass transfer within the adsorbent. Figure 2d shows two typical profiles, calculated using either the linear driving force (LDF) model or the Fickian diffusion model, which can be easily distinguished from one another.

Multiple steps of the described measurement protocol are performed until the desired equilibrium concentration is reached; each measurement step can be used to investigate the mass transfer on the adsorbent by analyzing the pressure profile. However, the pressure profile can be influenced by several other factors in addition to the mass transfer kinetics in the sorbent, such as heat transfer effects, instrument resistances, and bed effects.[35] While these effects can be included in the model used to analyze the experimental results, the first approach should be refining the measurement procedure to make them negligible, as modeling additional

https://doi.org/10.1021/acs.iecr.4c04099
Ind. Eng. Chem. Res. 2025, 64, 2339−2353

effects makes the model more complex, dependent on more parameters, and potentially less accurate.[35]

Refinement of the Measurement Procedure. The measurement procedure can be designed to reduce the effect of any factor other than the mass transfer kinetics on the pressure profile, and to quantify those that cannot be neglected so that they can be included in the sorption model. To this end, preliminary measurements were performed as suggested by Wang et al.,[35] with some adaptations where necessary.

First, heat transfer effects were investigated by using at least two different masses for each sorbent, and stainless steel beads were added to the measurement vial to increase the thermal mass. At the same time, this allows seeing any bed effect. Second, the amplitude of the pressure steps was varied to check whether a locally linear isotherm model could accurately describe equilibrium conditions. Wang et al.[35] suggest comparing adsorption with desorption measurements to check for this, though we found that this method cannot be directly applied to amine-functionalized materials due to the hysteresis of the CO_2 isotherm caused by the high heat of adsorption.[7] Third, the effect of instrument resistances was analyzed by performing blank measurements, i.e., without any adsorbent in the vial. When the dosage valve is opened, the gas must flow through the system to reach the adsorbent. In the case of fast-diffusing materials, resistances in the device may become limiting, hence need to be accounted for in the model.[35,38]

The preliminary measurements performed confirmed that adsorption occurred under isothermal conditions and was free of any bed effects, thus allowing for the assumption of steady temperature and negligible bed effects during the measurements. However, the use of a locally linear isotherm could not be justified even when reducing the amplitude of the pressure steps. Furthermore, blank measurements showed a significant contribution of instrument resistances. The latter two effects were therefore included in the mathematical model that is described in a later section.

Sorption Modeling. The sorption models were chosen based on the preliminary measurements, on experimental observations of the mass transfer in this work, and on observations made in literature for similar amine-functionalized sorbents. For all sorbents, two distinct phases of mass transfer were observed: the fast mass transfer phase is assumed to be due to pore diffusion, while the slow mass transfer phase is assumed to be due to diffusion within the amine layer. In all cases, the slow phase could be qualitatively described by the diffusion model. For the pore diffusion phase, two situations were observed and are qualitatively shown in Figure 2d. The profile of a surface resistance limited sorbent is a straight line after the equilibration between dosage and uptake cell, as observed for the TRI@unimodal pellets. The profile of a diffusion limited sorbent is a concave curve that converges to an asymptote,[38] as observed for both the TRI@bimodal pellets and the TRI@monolith. Based on these observations, two established mass transfer models were chosen to describe the two cases: a surface resistance model with internal diffusion for the TRI@unimodal pellets, and two diffusional resistances model for the TRI@bimodal and the TRI@monolith adsorbents.[19]

Adsorption Equilibrium. An equilibrium relation is required in both models for the boundary condition, and is described by a Toth model[18]

$$q_{CO_2}(P_{CO_2}) = \frac{q_s b P_{CO_2}}{[1 + (bP_{CO_2})^t]^{1/t}} \tag{2}$$

where P_{CO_2} is the partial pressure of CO_2, q_s is the saturation capacity, b is the affinity coefficient, and t is a parameter describing the heterogeneity of adsorption sites. The temperature dependency of the parameters is neglected, as a separate isotherm was fitted to each measurement to ensure good alignment between the model and the measurements, and the estimated parameters are provided in Table S3.

Surface Resistance with Internal Diffusion. The internal diffusional resistance is described using Fickian diffusion[19]

$$\frac{\partial q}{\partial t} = \frac{1}{r^2}\frac{\partial}{\partial r}\left(r^2 D_c \frac{\partial q}{\partial r}\right) \tag{3}$$

where q is the uptake in the solid, r is the radial coordinate in the microparticle, and D_c is the diffusion coefficient of CO_2 in the microparticle. The surface resistance is introduced through the relevant boundary condition, giving

$$D_c \left.\frac{\partial q}{\partial r}\right|_{r=r_c} = \frac{\varepsilon_p r_c}{(1-\varepsilon_p)R_p} k_p (c_b - c_p^*(q(r_c))) = \frac{\varepsilon_p r_c}{(1-\varepsilon_p)R_p}\frac{k_p}{R_g T}(P_b - P_p^*(q(r_c))) \tag{4}$$

$$\left.\frac{\partial q}{\partial r}\right|_{r=0} = 0 \tag{5}$$

where r_c is the radius of the microparticle, ε_p is the porosity of the sorbent, R_p is the radius of the pellet, k_p is the mass transfer coefficient associated with the surface resistance, c_b is the concentration in the bulb, and c_p^* is the concentration at equilibrium with the uptake at the surface of the microparticle. The geometric factor $\varepsilon_p r_c/((1-\varepsilon_p)R_p)$ accounts for the difference in the surface area of the pellet and that of the microparticles, through which the CO_2 molar flow must be the same.

Two Diffusional Resistances. In the original two diffusional resistances model, the internal resistance is described using eq 3 and the boundary condition (given above by eq 4) can be written as

$$q(r_c, t) = q^*(c_p) \tag{6}$$

The macropore diffusion is described by the following material balance in the macropores[19]

$$\frac{\partial c_p}{\partial t} + \left(\frac{1-\varepsilon_p}{\varepsilon_p}\right)\frac{\partial \overline{q}}{\partial t} = \frac{1}{R^2}\frac{\partial}{\partial R} R^2 D_p \frac{\partial c_p}{\partial R} \tag{7}$$

where c_p is the concentration in the pores of the sorbent, R is the radial coordinate of the pellet, and D_p is the diffusion coefficient within the pores. The average uptake $\overline{q}$ is calculated using

$$\overline{q}(c_p, t) = \frac{3}{r_c^3}\int_0^{r_c} q(r, c_p, t) r^2 \mathrm{d}r \tag{8}$$

We modify this model assuming the existence of two different adsorption sites,[21] with corresponding uptakes q_1 and q_2. Type 1 sites are the amine adsorption sites at the surface of

https://doi.org/10.1021/acs.iecr.4c04099
Ind. Eng. Chem. Res. 2025, 64, 2339−2353

the amine layer and are therefore not affected by internal diffusion, while type 2 sites are within the amine layer, and are reached by adsorbate molecules through internal diffusion. A constant parameter η is introduced to describe the fraction of surface sites, which is estimated using the adsorption rate measurements

$$q_1^* = \eta q^*,\ q_2^* = (1-\eta)q^* \text{ and } q = q_1 + q_2 \tag{9}$$

Equation 7 then becomes

$$\varepsilon_p \frac{\partial c_p}{\partial t} + (1-\varepsilon_p)\left(\frac{\partial \bar{q}_1}{\partial t} + \frac{\partial \bar{q}_2}{\partial t}\right) = \varepsilon_p \frac{1}{R^2}\frac{\partial}{\partial R} R^2 D_p \frac{\partial c_p}{\partial R} \tag{10}$$

where $\bar{q}_1 = q_1 = q_1^*$, as type 1 sites are assumed to be in instantaneous equilibrium with the gas and therefore only a function of c_p; this term can be dealt with in the same manner as with pure macropore diffusion control[19]

$$\frac{\partial q_1}{\partial t} = \frac{\mathrm{d}q_1^*}{\mathrm{d}c_p}\frac{\partial c_p}{\partial t} = \eta \frac{\mathrm{d}q^*}{\mathrm{d}c_p}\frac{\partial c_p}{\partial t} \tag{11}$$

The internal diffusional resistance in eq 3 then only applies to q_2. Taking the time derivative of eq 8, and using eq 3, one obtains

$$\frac{\partial \bar{q}_2}{\partial t} = \frac{3}{r_c} D_c \frac{\partial q_2}{\partial r}\bigg|_{r=r_c} \tag{12}$$

Substituting both eqs 11 and 12 into 10 yields

$$\frac{\partial c_p}{\partial t} = \frac{\varepsilon_p}{\varepsilon_p + (1-\varepsilon_p)\eta\frac{\mathrm{d}q^*}{\mathrm{d}c_p}}\left[\frac{1}{R^2}\frac{\partial}{\partial R} R^2 D_p \frac{\partial c_p}{\partial R} - \frac{(1-\varepsilon_p)}{\varepsilon_p}\frac{3}{r_c} D_c \frac{\partial q_2}{\partial r}\bigg|_{r=r_c}\right] \tag{13}$$

$$\frac{\partial q_2}{\partial t} = \frac{1}{r^2}\frac{\partial}{\partial r}\left(r^2 D_c \frac{\partial q_2}{\partial r}\right) \tag{14}$$

With the corresponding boundary conditions

$$c_p(R_p, t) = c_b = \frac{P_b}{R_g T}; \qquad \frac{\partial c_p}{\partial R}\bigg|_{R=0} = 0 \tag{15}$$

$$q_2(r_c, t) = q_2^*(c_p) = (1-\eta)q^*(c_p); \qquad \frac{\partial q_2}{\partial r}\bigg|_{r=0} = 0 \tag{16}$$

The initial conditions of a measurement step i are defined by the equilibrium condition of the previous measurement step

$$q_{i,0} = q_{i-1,\infty} \text{ and } c_{p,i,0} = c_{p,i-1,\infty} \tag{17}$$

For the two diffusional resistance model, the initial conditions for eq 14 are given by

$$q_{2,i,0} = (1-\eta)q_{i-1,\infty} \tag{18}$$

The geometry of the TRI@monolith pieces is slab-like, with alumina particles deposited within the macropores. The pore diffusion in TRI@monolith was therefore modeled in Cartesian coordinates.

Instrument Modeling. The boundary conditions in the sorption models described in the previous section are defined using the pressure P_b in the bulb of the vial. Due to the instrument resistances identified previously, this quantity is not necessarily equal to the pressure measured in the dosage cell P_d, so a mathematical model of the device shown in Figure 1 was developed to determine P_b as a function of time. The device is divided into four volumes according to the three potential resistances: the dosage valve, the particle filters, and the neck of the vial. The dosage valve and particle filters are assumed to have negligible volumes compared to the rest of the system hence they are modeled using a mass transfer coefficient, while the resistance in the vial neck is modeled using Fick's law. The area of the dosage valve and of the filter are unknown and difficult to measure accurately, so we lump the mass transfer coefficients and the areas into one coefficient as follows: $\bar{k}_{valve} = k_{valve}A_{valve}$ and $\bar{k}_{filter} = k_{filter}A_{filter}$. Both lumped coefficients require estimation by fitting to experiments. The area of the vial A_{vial} is known, so no lumping of parameters is required there.A mole balance of the four volumes is performed, with the inlet and exhaust valve defining the system boundaries, and each volume is modeled as a well-stirred volume except the vial neck, where transport occurs via diffusion. The device is assumed to be isothermal; though this is not strictly the case during the measurements, a sensitivity analysis using a nonisothermal model showed little to no effect of the temperature on the results, therefore the simpler isothermal model was used. The resulting equations are

$$\frac{V_d}{R_g T}\frac{\mathrm{d}P_d}{\mathrm{d}t} = -J_{valve} = -\bar{k}_{valve}\frac{(P_d - P_u)}{R_g T} \tag{19}$$

$$\frac{V_u}{R_g T}\frac{\mathrm{d}P_u}{\mathrm{d}t} = J_{valve} - J_{filter} = \bar{k}_{valve}\frac{(P_d - P_u)}{R_g T} - \bar{k}_{filter}\frac{(P_u - P_v|_{z=0})}{R_g T} \tag{20}$$

$$\frac{1}{R_g T}\frac{\partial P_v}{\partial t} = -\frac{\partial}{\partial z} j_{vial} = \frac{D_v}{R_g T}\frac{\partial^2 P_v}{\partial z^2} \tag{21}$$

$$\frac{V_b}{R_g T}\frac{\mathrm{d}P_b}{\mathrm{d}t} = J_{vial}|_{z=l} - J_{sorb} = -\frac{D_v}{R_g T}\frac{\partial P_v}{\partial z}\bigg|_{z=l} - J_{sorb} \tag{22}$$

where V is the volume, T is the temperature, J the molar flow, j the molar flux, and D the diffusion coefficient of the corresponding compartments. For the surface resistance with internal diffusion model, the flow into the sorbent is defined as

$$J_{sorb} = k_p \varepsilon_p A_{sorb}(c_b - c_p^*) = \frac{k_p \varepsilon_p A_{sorb}}{R_g T}(P_b - P_p^*) \tag{23}$$

For the modified two diffusional resistance model, the flow is

$$J_{sorb} = -A_{sorb} D_p \frac{\partial c_p}{\partial R}\bigg|_{R=R_p} = -\frac{3V_{sorb}}{R_p R_g T} D_p \frac{\partial P_p}{\partial R}\bigg|_{R=R_p} \tag{24}$$

For blank measurements with no sorbent, the molar flow into the sorbent is $J_{sorb} = 0$. The initial conditions of eqs 19−22 are given by

$$P_d = P_{d,0} \text{ at } t = 0 \tag{25}$$

https://doi.org/10.1021/acs.iecr.4c04099
Ind. Eng. Chem. Res. 2025, 64, 2339−2353

$$P_u = P_v = P_b = P_{u,0} \text{ at } t = 0 \tag{26}$$

The boundary conditions for eq 21 are

$$-\frac{D_v}{R_g T}\frac{dP_v}{dz}\bigg|_{z=0} = \frac{\overline{k}_{filter}}{A_{vial} R_g T}(P_u - P_v|_{z=0}) \tag{27}$$

$$P_v|_{z=L} = P_b \tag{28}$$

At the low pressures used in this work, the diffusion along the neck of the vial is expected to be in the transition regime between Knudsen diffusion and Poiseuille flow, as shown in Figure S2. The diffusion coefficient along the vial neck D_v is estimated by using a combination of Knudsen diffusion D_K and Poiseuille flow D_{vis}, as provided by the following relation[19]

$$D_v = D_K + D_{vis} = 97\frac{d_v}{2}\sqrt{\frac{T}{M}} + \frac{P_{v,\infty} d_v^2}{32\mu} \tag{29}$$

where $P_{v,\infty}$ is the pressure reached at the end of the measurement step and d_v is the diameter of the vial. This represents a rather conservative estimate for the diffusion coefficient, as the pressure used in D_{vis} is in fact higher during the measurement and the contribution of viscous flow is generally underestimated when using the Poiseuille flow correlation in the transition regime.[18]

The system of equations above are solved numerically by discretizing the spatial derivatives using the finite volume method.[43] The resulting system of ordinary differential equations (ODEs) was then solved in Matlab using a built-in ODE solver ode15s.

Parameter Estimation. *Pore Diffusion Coefficient.* Many well-established correlations exist to calculate the diffusion coefficients in the pores of an adsorbent. The choice of correlation is based on the diffusion mechanisms contributing to the mass transfer within the adsorbent and can include Poiseuille diffusion, molecular diffusion, Knudsen diffusion, and surface diffusion.[20] Due to the high heat of adsorption on amine-functionalized adsorbents, we assume that the contribution of surface diffusion is negligible. Furthermore, due to the use of pure CO_2 in the measurements, no molecular diffusion occurs. We therefore assume a combination of Poiseuille and Knudsen diffusion, using eq 29 as a function of d_{pore} and the pressure P_b, instead of the vial diameter and the vial pressure, to describe the diffusion in the pores. The size of d_{pore} in a real porous solid is generally a distribution rather than a single value. To account for this, an average diffusion coefficient is calculated for each pore size range by using the parallel pore model.[19] The average pore diffusion coefficient for each pore size range $d_1 - d_2$ is defined as

$$\overline{D}_{p,d_1-d_2} = \frac{1}{\varepsilon_{d_1-d_2}}\int_{d_1}^{d_2} D(d_{pore}) f(d_{pore}) \mathrm{d}d_{pore} \tag{30}$$

The diffusion coefficient of the mesopores $D_{p,meso}$ was calculated using the range 2−50 nm according to the IUPAC classification.[41,44] For the calculation of the diffusion coefficient of the macropores $D_{p,macro}$, small volume fractions at large pore sizes lead to unrealistically high diffusion coefficients. Therefore, the range was adjusted according to the material and defined as 50 nm to 2 μm for TRI@bimodal, and 50 nm to 50 μm for TRI@monolith. The porosity $\varepsilon_{d_1-d_2}$ represents either the mesoporosity or the macroporosity, respectively. The function $f(d_{pore})$ is the probability that the pore size is in the interval d_{pore} to $d_{pore} + \mathrm{d}d_{pore}$.[19]

Characteristic Dimensions. The model uses spherical coordinates, while the pellets used in this work are cylindrical. For the modeling, an equivalent radius was calculated as the radius of a spherical particle having the same external surface to volume ratio as the pellets.[19] The monoliths are modeled as slabs, and the characteristic diffusion length is defined as half the wall thickness.

The characteristic dimension for micropore diffusion is more challenging to define. In this work, we calculate two possible diffusion lengths: the size of the alumina nanoparticles and the thickness of the amine layer. The size of the alumina nanoparticles is estimated using XRD measurements and the Scherrer equation.[45] Further information on this calculation is provided in the Supporting Information.

The thickness of the amine layer is estimated by assuming the layer is uniform across the whole internal surface area of the sorbent with a constant thickness, z_{amine}, as

$$z_{amine} = \frac{v_{amine}}{a_{amine}} \tag{31}$$

The specific volume of the amine layer, v_{amine}, can be estimated using the difference in pore volume of functionalized and nonfunctionalized sorbent measured by mercury intrusion. The specific area of the layer, a_{amine}, is assumed to be the average of the BET surface area of the functionalized and nonfunctionalized sorbent.

Fitting Procedure. The measurement device used here samples the pressure with varying frequency, so to avoid a bias of the fits toward areas with more sampling points, a spline was fitted to the measurements and sampled every second. A cutoff was defined using a normalized uptake[35]

$$\frac{\overline{q} - q_0}{q_\infty - q_0} = \frac{P_d - P_0}{P_\infty - P_0} \tag{32}$$

where P_0 is the theoretical pressure after an instantaneous equilibration between dosage and uptake cell. Measurement points between 0 and 0.95 of the normalized uptake were used for fitting, as later points were found to be susceptible to measurement errors of the final pressure P_∞. For measurements partially influenced by instrument resistances, the specific start and end times were defined to only include the sorbent mass transfer limited regime.

The normalized pressure ψ_d was used to fit the kinetic parameters using the sum of normalized square residuals as the following objective function

$$SS_n(\Phi)^2 = \sum_{i=1}^{N}\left(\frac{\psi_d(t_i) - \hat{\psi}_d(\Phi, t_i)}{\psi_d(t_i)}\right)^2 \tag{33}$$

where Φ denotes the kinetic coefficient(s) of the corresponding model. The function was minimized using the Matlab function lsqnonlin.

Experimental Campaign. An experimental campaign was performed to investigate the different mass transfer mechanisms. Measurements were performed at different temperatures between −15 and 45 °C on the structured adsorbents to investigate the effect on pore diffusion. Pore diffusion was found to be significant in the pellets, therefore their size was reduced in two steps to 0.9 and 0.08 mm to enable an investigation of the amine diffusion. For the monoliths, pore

https://doi.org/10.1021/acs.iecr.4c04099
Ind. Eng. Chem. Res. 2025, 64, 2339−2353

diffusion was found to be negligible and no size reduction was necessary.

RESULTS AND DISCUSSION

First, we present the results related to the material characterization in terms of pore size, pore volumes, and diffusion lengths as these provide the adsorbent parameters required for the modeling and the analysis of the kinetic results. The model is then validated against experimental results and used to analyze both pore diffusion and amine diffusion for all adsorbents. We conclude by providing a simplified model using the parameters obtained here for use in larger breakthrough or process models.

MATERIAL CHARACTERIZATION

Pore Size. Mercury intrusion measurements provide important information on both the pore volume and the pore size distribution of the adsorbents. The results are presented in Figure 3, showing a bimodal pore size distribution

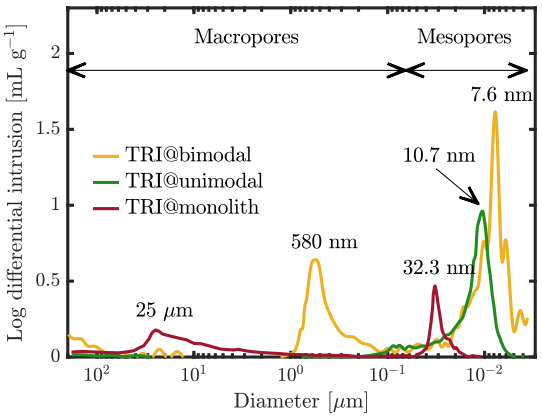

Figure 3. Pore size distributions of amine-functionalized materials using Hg porosimetry.

for both TRI@monolith and TRI@bimodal, and an unimodal pore size distribution for TRI@unimodal. The mesopores in both TRI@bimodal and TRI@unimodal are relatively similar in size, while those in TRI@monolith are significantly larger. Similarly, the macropores in TRI@monolith are significantly larger than those in TRI@bimodal. From eq 29 one sees that larger pores lead to faster diffusion; a bimodal pore size distribution can therefore significantly reduce diffusional resistance in the pores while maintaining a large surface area in the mesopores. The results of the mercury intrusion measurements are summarized together with those of the other characterization measurements in Table S2. N_2 physisorption measurements give similar estimates of the mesopore size as the mercury intrusion measurements using the BJH correlation, though the macropores cannot be captured using this technique.

Pore Volume. Comparing the pore volumes shows a significant difference between the adsorbents, which is reflected in the density and the porosity. For TRI@monolith, most of the porosity comes from the macropores that are present in the mullite skeleton, while the mesopore volume is given by the γ-alumina wash-coat. Given that γ-alumina makes up only ca. 10 wt % of TRI@monolith, the mesopore volume is significantly lower than that of both pellets. Consequently, the BET surface area of TRI@monolith is ca. 10% that of the pellets.

Diffusion Lengths. The diffusion length R_p is the characteristic length of the pore diffusion, and is very similar for both pellets, while significantly smaller for TRI@monolith. The characteristic length r_c for the micropore diffusion is more challenging to define. XRD measurements, shown in Figure S3, were used to determine the crystal size and revealed typical profiles observed for γ-alumina.[46,47] The small crystal sizes measured confirm that the γ-alumina is made up of clusters of nanoparticles.[46] The size of the nanoparticles is unlikely to be the diffusion length experienced by the CO_2, which would more likely diffuse through the clusters of nanoparticles that form the structure of the γ-alumina. Another characteristic length that could be used for the micropore diffusion is the thickness of the amine layer, z_{amine}. This is estimated assuming the amines are deposited in an even layer over the surface of the alumina nanoparticles. Both characteristic lengths are similar in magnitude, so the thickness of the amine layer was chosen for use in the model, as this aligns with the assumption that the slow diffusion mechanism is diffusion through the amine layer. Assuming it is coated on the nanoparticles and the length scales are very similar, the use of radial coordinates for the micropore diffusion is justified. It should be noted that the assumption of an even amine layer is strong—in reality it is likely quite heterogeneous. Note that the choice of characteristic length will affect the absolute value of the diffusion coefficient D, while the ratio D/r^2 will remain constant regardless of the characteristic length chosen. Based on the properties given in this section, the pore diffusion in TRI@monolith is expected to be very fast due both to the large macropores and to the short characteristic length. The pore diffusion in TRI@bimodal is likely significantly slower than TRI@monolith, though faster than in TRI@unimodal. Based on the estimated amine layer thickness, the diffusion in the amine layer is expected to be slowest in TRI@monolith, and similar for the pellets.

Model Validation. The model developed in this work is validated using measurements carried out in three limiting cases. First, blank measurements are used to measure the instrument resistances. Second, a fast diffusing adsorbent (TRI@monolith) is used to validate the estimated resistances in the presence of an adsorbent. Third, the model is fitted to measurements with the three sorbents to verify that the sorption models can indeed describe mass transfer. The instrument values used in the model are given in the Supporting Information in Table S1.

Blank Measurements. Measurements were performed using three vial configurations to elucidate the instrument resistances, and to inform the choice of vial configuration for adsorption measurements:

1. Standard vial (length of neck 230 mm) with glass rod and removable particle filter—this is the standard configuration recommended by the manufacturer.
2. Standard vial without glass rod and removable particle filter—this reduces both the filter resistance and diffusional resistance in the vial neck.
3. Shortened vial (length of neck 70 mm) without glass rod and removable particle filter—this further reduces the diffusional resistance in the vial neck. A significant difference to the second configuration would indicate

https://doi.org/10.1021/acs.iecr.4c04099
Ind. Eng. Chem. Res. 2025, 64, 2339−2353

that the rate-limiting resistance is the diffusion in the vial neck.

An example of a measurement and of the corresponding fit is shown in Figure 4, where two regimes of pressure decay can be

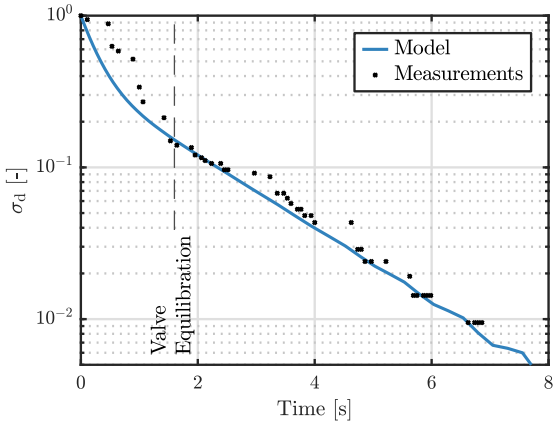

Figure 4. Normalized pressure profiles from a blank measurement using a vial without removable filter and without glass rod. Model fitted using eqs 19−22 without any sorbent (J_{sorb} = 0).

identified: the first regime lasts for ca. 2 s where the limiting resistance was identified as the dosage valve by observing P_u. The second regime lasts for another ca. 6 s, though here the limiting resistance cannot be identified directly as there are no further pressure sensors downstream; it could therefore be either in the vial neck or in the filters. Modeling the measurements with the diffusion coefficient in the vial determined using eq 29, a sensitivity analysis on $\overline{k}_{filter}$ revealed that the filter resistance is the limiting resistance.

Multiple measurements were performed for each vial configuration to determine $\overline{k}_{valve}$ and $\overline{k}_{filter}$; the values obtained are reported in Table 1 for each configuration together with

Table 1. Average Mass Transfer Coefficients Fitted to Blank Measurements Using Equations 19−22 for Different Vial Configurations

vial configuration	$\overline{k}_{valve} \times 10^5$ [m^3 s^{-1}]	$\overline{k}_{filter} \times 10^6$ [m^3 s^{-1}]
filter & rod	3.0 ± 0.7	2.0 ± 0.7
no filter and rod	2.9 ± 0.2	5.0 ± 1.0
shortened vial	3.3 ± 1.1	7.8 ± 8.7

the standard deviation of the measurements. The valve coefficient $\overline{k}_{valve}$ remains similar for all vial configurations, as expected, while $\overline{k}_{filter}$ increases significantly when one of the particle filters is removed. Using a shortened vial further increases the average $\overline{k}_{filter}$, though the uncertainty becomes very high due to large variations observed in the pressure profiles; it is unclear what the reason for this is. Based on these observations the standard vial with neither filter nor rod was chosen for the adsorption measurements, as it offers a good compromise between decreased instrument resistance and predictability. To check whether the removal of the rod has an adverse effect on the accuracy of the measurements, an isotherm was measured on TRI@bimodal both with and without a glass rod. The isotherms are identical within the error of the device, as shown in Figure S1.

Instrument Resistance Controlled Adsorption Measurements. It has been mentioned in literature that blank measurements should not be used to quantify instrument resistances as the flow during sorption measurements can far exceed that experienced during blank measurements.[38] The mass transfer coefficients obtained with blank measurements were therefore used to model adsorption measurements with partial instrument resistance limitation. Using the two diffusional resistance model, D_c was artificially increased to highlight the transition from adsorbent limited kinetics (convex profile) to instrument limited kinetics (straight profile). The results are shown in Figure 5, where the model

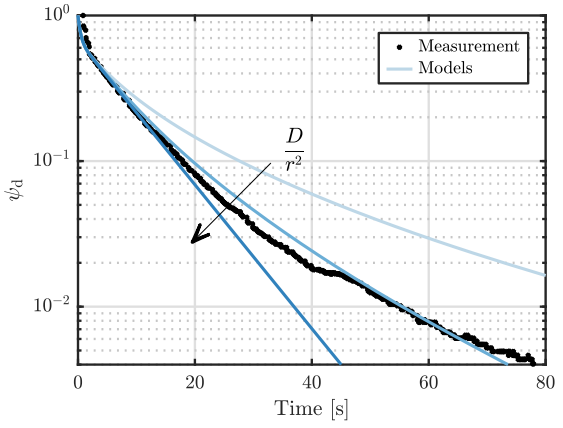

Figure 5. Effect of instrument resistances on an adsorption measurement demonstrated with the help of the diffusion model. Artificially increasing the diffusion coefficient in the model shows that the kinetics are instrument limited up to ca. 20 s (straight line), and sorbent limited thereafter (deviation from straight line).

clearly shows the region that is instrument resistance limited, i.e., between 0 and ca. 20 s, and the region that is adsorbent kinetics limited, i.e., after 20 s. The model fits the instrument resistance limited region well, confirming the values of the coefficients estimated through blank measurements. All measurements were checked using this method, and it was found that some fast diffusing systems were at least partially limited by the instrument resistances in the first measurement steps, thus recommending the inclusion of instrument resistances in the model.

Adsorbent Mass Transfer Controlled Measurements. The model was then fitted to the measurements of the structured sorbents at 25 °C, which are shown in Figure 6 for all three materials. The model gives a good fit for all the measurements, especially at the short to medium time scales, whereas small deviations can be observed at longer time scales. This is caused by two factors: the models are fitted to the measurement points only up to 0.95 relative uptake, and the variability of the measurement points increase at longer time scales due to errors of the pressure measurements.

Both the TRI@bimodal pellets and the TRI@monolith pieces can be well described by the two diffusional resistance model, as is shown in Figure 6b,c, respectively. The TRI@unimodal pellets are better described by the surface resistance with internal diffusion model as shown in Figure 6a, which is visible from the initial linear decrease of the pressure that is typical of a surface resistance. The necessity for models that describe two mass transfer resistances is especially visible in the case of the TRI@unimodal pellets, where the normalized

https://doi.org/10.1021/acs.iecr.4c04099
Ind. Eng. Chem. Res. 2025, 64, 2339−2353

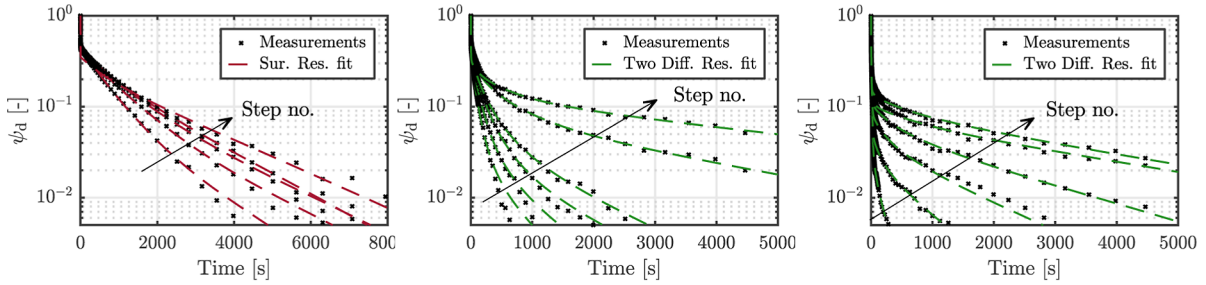

(a) TRI@unimodal. (b) TRI@bimodal. (c) TRI@monolith.

Figure 6. Model fits and experiments of multiple steps in a measurement series for all adsorbents at 25 °C. The surface resistance with internal diffusion model (sur. res.) was used for TRI@unimodal, and the two diffusional resistance model (two diff. res.) was used for both TRI@bimodal and TRI@monolith.

pressure profile deviates from the straight profile describing a pure surface resistance at longer time scales. This is due to the slow diffusion mechanism, assumed to be within the amine layer, and is consistent with literature describing mass transfer in similar amine-functionalized adsorbents.[5,21] While this observation is less obvious in the two diffusional resistance model, using a model with only one diffusional resistance we were unable to describe the whole pressure profile.

Pore Resistances. Three different pore diffusion situations were observed for the three adsorbents used in this work: for TRI@monolith, the pore diffusion is faster than the instrument resistances hence could not be measured, while for TRI@unimodal surface resistance was found to be limiting rather than pore diffusion. TRI@bimodal was found to be the only adsorbent of the three with measurable pore diffusion. In this section we discuss the pore diffusion in TRI@bimodal and the surface resistance observed in TRI@unimodal.

TRI@bimodal. The pore diffusion coefficients are calculated for TRI@bimodal using eq 30 and the results are reported in Table 2 together with the estimated pore diffusion coefficients $D_{p,est}$; the value is the average of all the measurement steps excluding outliers while the uncertainty is the standard deviation. Typically, pore diffusion coefficients calculated using correlations require modification with the tortuosity to account for the complexity of the pore structure in real sorbents.[18] This factor is calculated to be close to unity for TRI@bimodal using correlations[18] owing to the high porosity, and is therefore not accounted for.

Table 2. Pore Diffusion Coefficients of TRI@bimodal from Correlations and from Model Fits

temperature [K]	$D_{p,meso}$ [m^2 s^{-1}] × 10^6	$D_{p,macro}$ [m^2 s^{-1}] × 10^6	$D_{p,est}$ [m^2 s^{-1}] × 10^6
258	1.87	82	1.2 ± 0.4
268	1.90	84	2.1 ± 0.9
278	1.94	85	3.0 ± 0.8
288	1.97	87	4.3 ± 1.0
298	2.01	88	2.0 ± 0.6
308	2.04	90	5.5 ± 1.8
318	2.07	91	11 ± 4.9

The calculated values $D_{p,meso}$ and $D_{p,macro}$ exhibit a moderate dependence on temperature, as is the case for Knudsen diffusion, while the estimated values $D_{p,est}$ exhibit a stronger dependence. The discrepancy can indicate that the assumed pore diffusion mechanisms fail to describe the whole situation. The magnitude of the estimated coefficients indicates that the pore resistance occurs mainly in the mesopores rather than in the macropores.

TRI@unimodal. The mass transfer resistance in TRI@unimodal was observed to be on the surface rather than within the pores at short to medium time scales. The mass transfer coefficients describing this surface resistance are given in Table 3. In literature, specific geometric surface areas are often incorporated into the mass transfer coefficients, therefore we also provide the values of $k_{p,est}a_p$. These values are similar to those obtained by Stampi-Bombelli et al.[5] using breakthrough measurements on the same adsorbent and will be discussed in a later section.

Table 3. Fitted Pore Mass Transfer Coefficient for TRI@unimodal

temperature [K]	$k_{p,est}$ × 10^3 [m s^{-1}]	$k_{p,est}a_p$ [s^{-1}]
258	2.2 ± 1.3	2.5 ± 1.5
278	3.2 ± 1.0	3.7 ± 1.1
298	2.4 ± 0.7	2.7 ± 0.8

To further investigate the surface resistance, the pellets were successively crushed to 900 and 80 μm before measuring the adsorption kinetics. For both particle sizes, the surface resistance was no longer visible in the pressure profiles, thus confirming that the resistance is on the surface of the pellet. Measurements performed on nonfunctionalized pellets, shown in Figure S6, revealed the absence of a surface barrier, indicating that this is introduced through the grafting procedure.

Amine Diffusion. A qualitative assessment of the pressure profiles and of the asymptotes shown in Figure 6 give an indication of the development of the diffusion coefficient over the different measurement steps, with steeper asymptotes describing faster diffusion. The long time scales are generally controlled by amine diffusion, and the gradient of the asymptotes is shown to decrease with increasing step number for all adsorbents, thus indicating slowing diffusion with increasing uptake. To investigate this effect in further detail, TRI@bimodal and TRI@unimodal were crushed and sieved to 80 μm to eliminate pore diffusion effects. This was not necessary for TRI@monolith as pore diffusion was negligible. The estimated amine diffusion coefficients D_c of all adsorbents are plotted in Figure 7, and are shown to decrease as a function of the normalized uptake. This observation is consistent with a recent study by Vallace et al.[32] on mass transfer kinetics in various amine functionalized adsorbents. They postulated that the reaction between CO_2 and the amines causes cross-linking

https://doi.org/10.1021/acs.iecr.4c04099
Ind. Eng. Chem. Res. 2025, 64, 2339−2353

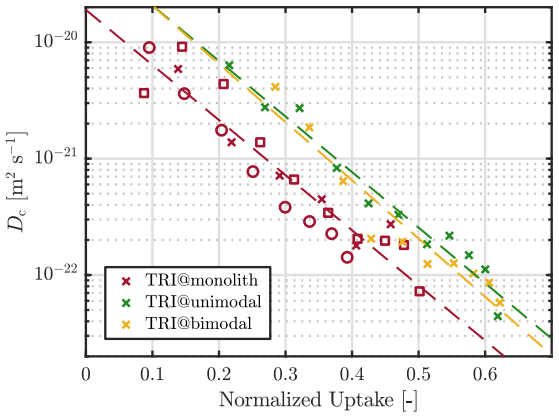

Figure 7. Effect of uptake on the amine diffusion coefficient of three adsorbents. The pellets were powdered to 80 μm to eliminate pore diffusion. The different symbols denote measurements done at different temperatures: □ = 258 K, ○ = 278 K, × = 298 K.

in the polymer which increases diffusional resistance. Measurements performed on powders in the same study matched the proposed model well and seemed to confirm the hypothesis, though no direct experimental evidence was provided, as the desired concentration (400 ppm) was reached in one measurement step. The estimated coefficients shown in Figure 7 seem to confirm the hypothesis. The mechanism is described by modifying a correlation given by Stendardo and Foscolo[32,48]

$$D_c = D_0 \exp\left(-\alpha\left(1 - \frac{C_{am}}{C_{am,0}}\right)^{\beta}\right) \tag{34}$$

where C_{am} describes the concentration of unreacted amines, α and β are empirical positive parameters, and D_0 is the diffusion coefficient of CO_2 in the amine layer with no adsorbed CO_2. We propose a modification of eq 34 to avoid the necessity of knowing the amine concentration in the solid, and of modeling it over time, by making the assumptions (1) that two amines are required to adsorb one CO_2 molecule, and (2) that all amine sites are available for adsorption. Therefore, the saturation capacity of the isotherm, q_s, is proportional to the initial amine concentration, i.e.

$$q_s = \frac{C_{am,0}}{2} \tag{35}$$

Using the first assumption, one can write

$$C_{am} = C_{am,0} - 2q = 2(q_s - q) \tag{36}$$

Substituting these correlations into eq 34 gives

$$D_c = D_0 \exp\left(-\alpha\left(\frac{q}{q_{s,Toth}}\right)^{\beta}\right) \tag{37}$$

The results of the fitting are shown in Figure 7, obtained with the coefficients given in Table 4. Comparing the values of $q_{s,Toth}$ with the amine contents provided in Table S2 indicates that assumption (2) is not fulfilled with the isotherms obtained here. As the isotherms are fitted to the low pressure range used in the kinetic measurements, this decreases the accuracy of the q_s value. In addition, not all amines will be available for adsorption on real adsorbents and the amine content will be underestimated using q_s as a proxy. However, only the amines available for adsorption are able to undergo cross-linking and the use of q_s would therefore arguably better describe the physical situation.

Table 4. Fitted Parameters Describing the Self-Limiting Amine Diffusion for the Adsorbents in This Work[a]

	TRI@bimodal	TRI@unimodal[b]	TRI@monolith
D_0 [m^2 s^{-1}]	6.5×10^{-20}	6.2×10^{-20}	1.9×10^{-20}
α [-]	11.5	11.0	10.9
β [-]	1	1	1
$q_{s,Toth}$ [mol kg^{-1}]	0.85	0.72	0.038
η [-]	0.41	0.42	0.26

[a]Fitted using the two diffusional resistance model, as this model provided a better fit for the powdered TRI@unimodal pellets. [b]Parameter β is not fitted to the measurements as it is observed to be close to unity.

The decrease in diffusion coefficients shown in Figure 7 is approximately linear on the semilogarithmic plot, so the exponent β is assumed to be equal to one for the fitting of D_0 and α. Qualitatively, D_0 describes the diffusion at zero uptake while α describes the rate of decrease in diffusivity due to the cross-linking of amines. It follows that D_0 is likely influenced by both the type of amines and the functionalization procedure, which in the case of wet grafting can influence the extent of amine polymerization.[40,49] The coefficient α is likely influenced by the type of amines only, as the cross-linking mechanism that causes the decrease in diffusivity should remain the same for the same amines, regardless of the extent of polymerization. Accordingly, the value of α is very similar for all three adsorbents measured in this work. The value of D_0 is very similar for both TRI@unimodal and TRI@bimodal, though there appears to be a higher mass transfer resistance in the amine layer on TRI@monolith, as indicated by a lower value of D_0. Larger pores have been reported to enable higher degrees of amine polymerization,[50] which is plausibly the case for TRI@monolith given its larger mesopores. This is further underlined by the lower fraction of surface sites η in TRI@monolith. Interestingly, the fraction of surface sites η is less than half of the total amine sites for all materials. As mass transfer kinetics are key to improving the productivity of DAC operations,[9,11] these values provide valuable insight for improving DAC sorbents.

The estimates of the diffusion coefficient D_c in Figure 7 do not seem to be affected by the temperature when plotted against the normalized uptake. This indicates that the effect of temperature on the amine diffusion coefficient is accounted for in the saturation capacity $q_{s,Toth}$.

Application to Breakthrough and Process Modeling. The models introduced previously offer an accurate description of the measurements and are therefore useful for obtaining good estimates of the diffusion coefficients. However, they are too computationally expensive for use in larger process models and are often replaced by simpler models, such as the pseudo first order linear driving force (LDF) model[51]

$$\frac{\partial q}{\partial t} = k(q^* - q) \tag{38}$$

where the mass transfer coefficient k has the units s^{-1} and includes the specific geometric surface area. Diffusion coefficients such as those obtained in this work can be used

https://doi.org/10.1021/acs.iecr.4c04099
Ind. Eng. Chem. Res. 2025, 64, 2339−2353

Table 5. Summary of Kinetic Coefficients at 25 °C Estimated in This Work for Use in Process Models[d]

parameter	TRI@monolith		TRI@unimodal		TRI@bimodal
	this work	ref 5	this work	ref 5	this work
k_g [s^{-1}]	[a]	67	2.7[b]	2.79	12.6
$\bar{k}_{amine}$ [s^{-1}]	1.1×10^{-3}	1.1×10^{-3}	2.0×10^{-3}	[c]	4.4×10^{-3}
$k_{amine,0}$ [s^{-1}]	0.016		0.19		0.35
η [-]	0.26	0.75	0.42	[c]	0.41

[a]Pore diffusion in TRI@monolith could not be measured here. [b]The value $k_{p,est}a_p$ from Table 3 is used here. [c]No η or $k_{s,amine}$ could be fitted. [d]Coefficients estimated using breakthrough measurements are provided for comparison, reproduced from Stampi-Bombelli et al.[5]

in this model through the relations given by Glueckauf and Coates[52]

$$k_g = \frac{15\varepsilon_p D_{p,est}}{R_p^2} \tag{39}$$

where k_g is used to describe mass transfer in the gas phase. To describe mass transfer in the amine phase, one can define the mass transfer coefficient k_{amine}

$$\begin{aligned} k_{amine} &= \frac{15D_c}{r_c^2} \\ &= \frac{15D_0}{r_c^2}\exp\left(-\alpha\frac{q}{q_{s,Toth}}\right) \\ &= k_{amine,0}\exp\left(-\alpha\frac{q}{q_{s,Toth}}\right) \end{aligned} \tag{40}$$

assuming $\beta = 1$. However, eq 38 cannot describe both mechanisms at once, and a modification has been shown to give good results in the modeling of breakthrough measurements[5,21,22]

$$\frac{\partial q_1}{\partial t} = k_1(\eta q^* - q_1) \tag{41}$$

$$\frac{\partial q_2}{\partial t} = k_2((1-\eta)q^* - q_2) \tag{42}$$

$$q = q_1 + q_2 \tag{43}$$

These correlations are based on the same principles used to derive the mass transfer equations in this work, and the relation of the different adsorption sites is identical to eq 9. The mass transfer coefficients are defined as[5,22]

$$\frac{1}{k_1} = \frac{1}{k_g}\frac{q^*_{p,in}}{c_{in}} + \frac{1}{k_s} \tag{44}$$

$$\frac{1}{k_2} = \frac{1}{k_1} + \frac{1}{k_{amine}} \tag{45}$$

where k_g describes the mass transfer in the gas phase, k_s describes the mass transfer in the solid phase except for in the amine phase, and k_{amine} describes the diffusion in the amine phase. Note that in this work we assume the mass transfer in the solid phase to be negligible, therefore $k_s = 0$. Due to the absence of film resistances when using pure CO_2, k_g only describes the pore diffusion or surface resistance.

The coefficients calculated using eqs 39 and 40 are given in Table 5, and compared to those obtained for the same materials TRI@unimodal and TRI@monolith using breakthrough measurements, whose detailed analysis is reported by Stampi-Bombelli et al.[5] To enable a comparison of k_{amine} with the breakthrough results, an average of the amine coefficients $\bar{k}_{amine}$ is provided. The mass transfer coefficients k_g for TRI@unimodal and $\bar{k}_{amine}$ for TRI@monolith are shown to align well with those of the breakthrough measurements. A deviation of the obtained values of η is observed for TRI@monolith, which may be attributed to the difference in measurement method. Breakthrough measurements include many effects such as axial dispersion, convection, heat transfer, and mass transfer in the sorbent, and it may be challenging to deconvolute each effect. Volumetric measurements offer the possibility to directly quantify just the mass transfer in the adsorbent itself when modeled correctly. This is underlined by the ability to measure k_{amine} and η for TRI@unimodal, which was not possible using breakthrough measurements. The values of η obtained here correspond well to values obtained in literature for similar adsorbents.[21] The mass transfer coefficients obtained for TRI@bimodal indicate a significant improvement of pore diffusion over TRI@unimodal, as is expected for such a bimodal pore size distribution, though they are still significantly below that of TRI@monolith.The limitations of the piezometric method with the device used here are evident from its inability to obtain a gas diffusion coefficient k_g for TRI@monolith. In addition, mass transfer resistances relating to mixtures of gases such as film diffusion are not evaluated as only pure gases are used. These factors should be taken into consideration when using mass transfer coefficients obtained using the piezometric method.

CONCLUSIONS

In this work, we used of a commercial volumetric device to measure the mass transfer kinetics of three amine functionalized alumina adsorbents with varying pore structures. A model was developed to quantify the mass transfer resistances within the adsorbents, with the goal (1) of providing a framework for the use of commercial volumetric devices to measure mass transfer kinetics, and (2) of quantifying the limiting mass transfer mechanisms in three structured amine functionalized adsorbents. In doing so, we gained the following valuable insights.

- Mass transfer resistances in the device can be accounted for in the boundary condition of the adsorption models by modeling the device. Depending on the vial configuration and the pressure range of the measurement, the dosage valve, the particle filters and the vial neck can represent a significant mass transfer resistance.
- Both pore diffusion and diffusion within the amine layer play a significant role in the bimodal pellets, while a surface resistance introduced by the functionalization procedure dominates in the unimodal pellets. Only the

https://doi.org/10.1021/acs.iecr.4c04099
Ind. Eng. Chem. Res. 2025, 64, 2339−2353

diffusion within the amine layer could be measured in the monolith, due to significant instrument resistances masking the pore diffusion effects.

- In amine functionalized adsorbents where amine diffusion is at least partially limiting, the mass transfer model requires the use of two different adsorption sites to accurately describe the measurement data.
- Experimental proof is provided that diffusion in the amine layer is dependent on the uptake; a correlation proposed in the literature can adequately describe this phenomenon.
- The mass transfer parameters estimated in this work are shown to align well with those obtained using breakthrough experiments. Using the Glueckauf approximation, the values can be redefined as mass transfer coefficients for the computationally leaner two-site LDF model, and therefore be used in process models.
- Commercial piezometric devices are limited in measuring very fast mass transfer due to instrument resistances, which can be identified if the instrument resistances are quantified and modeled.

■ ASSOCIATED CONTENT

Supporting Information

The Supporting Information is available free of charge at https://pubs.acs.org/doi/10.1021/acs.iecr.4c04099.

Additional information on the modeling methods and material characterization (PDF)

■ AUTHOR INFORMATION

Corresponding Author

Marco Mazzotti − *Institute of Energy and Process Engineering, ETH Zurich, Zurich 8092, Switzerland;* orcid.org/0000-0002-4948-6705; Email: marco.mazzotti@ipe.mavt.ethz.ch

Author

Quirin Grossmann − *Institute of Energy and Process Engineering, ETH Zurich, Zurich 8092, Switzerland;* orcid.org/0000-0003-0999-0891

Complete contact information is available at: https://pubs.acs.org/10.1021/acs.iecr.4c04099

Notes

The authors declare no competing financial interest.

■ ACKNOWLEDGMENTS

This work was funded by the Swiss National Science Foundation grant number 197221. We also thank Andreas Klimera from HUG Engineering for providing the many wash-coated monoliths, as well as Saint Gobain for the alumina pellets and Sasol for providing the wash-coat. We also warmly thank Merlin Hosner for his contribution to the early stage of this work and Prof. Dr. Ronny Pini for the insightful discussions.

■ NOTATION

Roman Symbol

a	specific area [$m^2\ g^{-1}$]
A	area [m^2]
b	affinity coefficient of Toth isotherm [kPa^{-1}]
c	concentration [$mol\ m^{-3}$]
C_{am}	amine concentration [$mol\ m^{-3}$]
d	diameter [m]
D	diffusion coefficient [$m^2\ s^{-1}$]
j	molar flux [$mol\ m^{-2}\ s^{-1}$]
J	molar flow [$mol\ s^{-1}$]
$\overline{k}$	lumped mass transfer coefficient incl. area [$m^3\ s^{-1}$]
k	mass transfer coefficient [$m\ s^{-1}$]
L	length of vial neck [m]
M	molar mass [$kg\ mol^{-1}$]
P	pressure [Pa]
q	uptake [$mol\ m^{-3}$]
r	radial coordinate in the crystal/amine layer [m]
R_g	universal gas constant [$m^3\ Pa\ K^{-1}\ mol^{-1}$]
R	radial coordinate in the pellets [m]
t	time [s]
t	heterogeneity parameter of Toth isotherm [-]
T	temperature [K]
v	specific volume [$m^3\ g^{-1}$]
V	volume [m^3]
z	axial coordinate for diffusion along vial neck or within monolith wall [m]
z_{amine}	thickness of amine layer [m]

Greek Symbols

α	coefficient in eq 37 [-]
β	coefficient in eq 37 [-]
ϵ	porosity [-]
η	fraction of type 1 adsorption sites [-]
μ	viscosity [Pa s]
ρ	density [$kg\ m^3$]
ψ	normalized pressure [-]

Subscripts and Superscripts

*	equilibrium value
^	estimated
-	average
0	initial condition beginning of measurement step
1	type 1 adsorption sites
2	type 2 adsorption sites
∞	end of measurement step
b	uptake cell bulb
c	crystal
d	dosage cell
K	Knudsen
n	normalized
p	pellet
s	saturation or solid
sorb	sorbent
u	uptake cell device
v	uptake cell neck
vis	viscous

Acronyms

LDF	linear driving force
SS	sum of squared residuals

■ REFERENCES

(1) IPCC. *Climate Change 2022: Mitigation of Climate Change. Contribution of Working Group III to the Sixth Assessment Report of the Intergovernmental Panel on Climate Change*; Shukla, P., Skea, J., Slade, R., Khourdajie, A. A., van Diemen, R., McCollum, D., Pathak, M., Some, S., Vyas, P., Fradera, R., Belkacemi, M., Hasija, A., Lisboa, G., Luz, S., Malley, J., Eds.; Cambridge University Press, 2022.

(2) Deutz, S.; Bardow, A. Life-cycle assessment of an industrial direct air capture process based on temperature−vacuum swing adsorption. *Nat. Energy* **2021**, *6*, 203−213.
(3) Terlouw, T.; Bauer, C.; Rosa, L.; Mazzotti, M. Life cycle assessment of carbon dioxide removal technologies: a critical review. *Energy Environ. Sci.* **2021**, *14*, 1701−1721.
(4) Wurzbacher, J. A.; Gebald, C.; Steinfeld, A. Separation of CO_2 from air by temperature-vacuum swing adsorption using diamine-functionalized silica gel. *Energy Environ. Sci.* **2011**, *4*, 3584−3592.
(5) Stampi-Bombelli, V.; Storione, A.; Grossmann, Q.; Mazzotti, M. On Comparing Packed Beds and Monoliths for CO2 Capture from Air Through Experiments, Theory, and Modeling. *Ind. Eng. Chem. Res.* **2024**, *63*, 11637−11653.
(6) Stampi-Bombelli, V.; van der Spek, M.; Mazzotti, M. Analysis of direct capture of CO_2 from ambient air via steam-assisted temperature−vacuum swing adsorption. *Adsorption* **2020**, *26*, 1183−1197.
(7) Young, J.; García-Díez, E.; Garcia, S.; Van Der Spek, M. The impact of binary water-CO_2 isotherm models on the optimal performance of sorbent-based direct air capture processes. *Energy Environ. Sci.* **2021**, *14*, 5377−5394.
(8) Gelles, T.; Lawson, S.; Rownaghi, A. A.; Rezaei, F. Recent advances in development of amine functionalized adsorbents for CO_2 capture. *Adsorption* **2020**, *26*, 5−50.
(9) Young, J.; Mcilwaine, F.; Smit, B.; Garcia, S.; Van der Spek, M. Process-informed adsorbent design guidelines for direct air capture. *Chem. Eng. J.* **2023**, *456*, 141035.
(10) Low, M.-Y. A.; Barton, L. V.; Pini, R.; Petit, C. Analytical review of the current state of knowledge of adsorption materials and processes for direct air capture. *Chem. Eng. Res. Des.* **2023**, *189*, 745−767.
(11) Azarabadi, H.; Lackner, K. S. A sorbent-focused techno-economic analysis of direct air capture. *Appl. Energy* **2019**, *250*, 959−975.
(12) Climeworks Orca. the first large-scale plant. https://climeworks.com/plant-orca, 2021 (accessed March 21, 2024).
(13) Shi, X.; Xiao, H.; Azarabadi, H.; Song, J.; Wu, X.; Chen, X.; Lackner, K. S. Sorbents for the direct capture of CO_2 from ambient air. *Angew. Chem., Int. Ed.* **2020**, *59*, 6984−7006.
(14) Sanz-Pérez, E. S.; Murdock, C. R.; Didas, S. A.; Jones, C. W. Direct capture of CO_2 from ambient air. *Chem. Rev.* **2016**, *116*, 11840−11876.
(15) Wijesiri, R. P.; Knowles, G. P.; Yeasmin, H.; Hoadley, A. F.; Chaffee, A. L. CO_2 capture from air using pelletized polyethylenimine impregnated MCF silica. *Ind. Eng. Chem. Res.* **2019**, *58*, 3293−3303.
(16) Gebald, C.; Wurzbacher, J. A.; Tingaut, P.; Zimmermann, T.; Steinfeld, A. Amine-based nanofibrillated cellulose as adsorbent for CO_2 capture from air. *Environ. Sci. Technol.* **2011**, *45*, 9101−9108.
(17) Rezaei, F.; Webley, P. Structured adsorbents in gas separation processes. *Sep. Purif. Technol.* **2010**, *70*, 243−256.
(18) Do, D. D. *Adsorption Analysis: Equilibria and Kinetics*, Chapter Adsorption Analysis: Equilibria and Kinetics; World Scientific, 1998; pp 337−414.
(19) Kärger, J.; Ruthven, D. M.; Theodorou, D. N.; et al. *Diffusion in Nanoporous Materials*; Wiley Online Library, 2012; Vol. *48*.
(20) Ruthven, D. M. *Principles of Adsorption and Adsorption Processes*; John Wiley & Sons, 1984.
(21) Bollini, P.; Brunelli, N. A.; Didas, S. A.; Jones, C. W. Dynamics of CO_2 adsorption on amine adsorbents. 2. Insights into adsorbent design. *Ind. Eng. Chem. Res.* **2012**, *51*, 15153−15162.
(22) Kalyanaraman, J.; Fan, Y.; Lively, R. P.; Koros, W. J.; Jones, C. W.; Realff, M. J.; Kawajiri, Y. Modeling and experimental validation of carbon dioxide sorption on hollow fibers loaded with silica-supported poly(ethylenimine). *Chem. Eng. J.* **2015**, *259*, 737−751.
(23) Gelles, T.; Rezaei, F. Diffusion kinetics of CO_2 in amine-impregnated MIL-101, alumina, and silica adsorbents. *AIChE J.* **2020**, *66*, No. e16785.
(24) Bos, M. J.; Kreuger, T.; Kersten, S. R.; Brilman, D. W. Study on transport phenomena and intrinsic kinetics for CO_2 adsorption in solid amine sorbent. *Chem. Eng. J.* **2019**, *377*, 120374.
(25) Elfving, J.; Sainio, T. Kinetic approach to modelling CO_2 adsorption from humid air using amine-functionalized resin: Equilibrium isotherms and column dynamics. *Chem. Eng. Sci.* **2021**, *246*, 116885.
(26) He, L.; Fan, M.; Dutcher, B.; Cui, S.; Shen, X. d.; Kong, Y.; Russell, A. G.; McCurdy, P. Dynamic separation of ultradilute CO_2 with a nanoporous amine-based sorbent. *Chem. Eng. J.* **2012**, *189*−*190*, 13−23.
(27) Wang, S.; Li, Y.; Li, Z. Fast Adsorption Kinetics of CO_2 on Solid Amine Sorbent Measured Using Microfluidized Bed Thermogravimetric Analysis. *Ind. Eng. Chem. Res.* **2020**, *59*, 6855−6866.
(28) Ebner, A. D.; Gray, M. L.; Chisholm, N. G.; Black, Q. T.; Mumford, D. D.; Nicholson, M. A.; Ritter, J. A. Suitability of a solid amine sorbent for CO_2 capture by pressure swing adsorption. *Ind. Eng. Chem. Res.* **2011**, *50*, 5634−5641.
(29) Jung, W.; Park, J.; Lee, K. S. Kinetic modeling of CO_2 adsorption on an amine-functionalized solid sorbent. *Chem. Eng. Sci.* **2018**, *177*, 122−131.
(30) Shi, W.; Chen, S.; Xie, R.; Gonzalez-Diaz, A.; Zhang, X.; Wang, T.; Jiang, L. Bi-disperse adsorption model of the performance of amine adsorbents for direct air capture. *Chem. Eng. J.* **2024**, *496*, 154090.
(31) Ohs, B.; Krödel, M.; Wessling, M. Adsorption of carbon dioxide on solid amine-functionalized sorbents: A dual kinetic model. *Sep. Purif. Technol.* **2018**, *204*, 13−20.
(32) Vallace, A.; Ren, Y.; Jones, C. W.; Lively, R. P. Kinetic model describing self-limiting CO2 diffusion in supported amine adsorbents. *Chem. Eng. J.* **2023**, *472*, 144838.
(33) Hou, C.; Kumar, D. R.; Jin, Y.; Wu, Y.; Lee, J. J.; Jones, C. W.; Wang, T. Porosity and hydrophilicity modulated quaternary ammonium-based sorbents for CO_2 capture. *Chem. Eng. J.* **2021**, *413*, 127532.
(34) Goeppert, A.; Czaun, M.; May, R. B.; Prakash, G. K. S.; Olah, G. A.; Narayanan, S. R. Carbon Dioxide Capture from the Air Using a Polyamine Based Regenerable Solid Adsorbent. *J. Am. Chem. Soc.* **2011**, *133*, 20164−20167.
(35) Wang, J.-Y.; Mangano, E.; Brandani, S.; Ruthven, D. M. A review of common practices in gravimetric and volumetric adsorption kinetic experiments. *Adsorption* **2021**, *27*, 295−318.
(36) Wilkins, N. S.; Rajendran, A.; Farooq, S. Dynamic column breakthrough experiments for measurement of adsorption equilibrium and kinetics. *Adsorption* **2021**, *27*, 397−422.
(37) Brandani, S. Analysis of the piezometric method for the study of diffusion in microporous solids: isothermal case. *Adsorption* **1998**, *4*, 17−24.
(38) Brandani, S.; Brandani, F.; Mangano, E.; Pullumbi, P. Using a volumetric apparatus to identify and measure the mass transfer resistance in commercial adsorbents. *Microporous Mesoporous Mater.* **2020**, *304*, 109277.
(39) Crank, J. *The Mathematics of Diffusion*; Oxford University Press, 1979.
(40) Grossmann, Q.; Stampi-Bombelli, V.; Yakimov, A.; Docherty, S.; Copéret, C.; Mazzotti, M. Developing Versatile Contactors for Direct Air Capture of CO2 through Amine Grafting onto Alumina Pellets and Alumina Wash-Coated Monoliths. *Ind. Eng. Chem. Res.* **2023**, *62*, 13594−13611.
(41) Thommes, M.; Kaneko, K.; Neimark, A. V.; Olivier, J. P.; Rodriguez-Reinoso, F.; Rouquerol, J.; Sing, K. S. Physisorption of gases, with special reference to the evaluation of surface area and pore size distribution (IUPAC Technical Report). *Pure Appl. Chem.* **2015**, *87*, 1051−1069.
(42) Schumacher, R.; Karge, H. G. Thermodynamics and kinetics of adsorption of selected monoalkylbenzenes in H-ZSM-5. *J. Phys. Chem. B* **1999**, *103*, 1477−1483.
(43) Haghpanah, R.; Majumder, A.; Nilam, R.; Rajendran, A.; Farooq, S.; Karimi, I. A.; Amanullah, M. Multiobjective optimization of a four-step adsorption process for postcombustion CO_2 capture via finite volume simulation. *Ind. Eng. Chem. Res.* **2013**, *52*, 4249−4265.

https://doi.org/10.1021/acs.iecr.4c04099
Ind. Eng. Chem. Res. 2025, 64, 2339−2353

(44) Sing, K. S. Reporting physisorption data for gas/solid systems with special reference to the determination of surface area and porosity (Recommendations 1984). *Pure Appl. Chem.* **1985**, *57*, 603−619.
(45) Cullity, B.; Stock, S. *Elements of X-ray Diffraction*, Chapter Diffraction III: Real Samples; Pearson, 2014; pp 171−191.
(46) Chaikittisilp, W.; Kim, H.-J.; Jones, C. W. Mesoporous alumina-supported amines as potential steam-stable adsorbents for capturing CO_2 from simulated flue gas and ambient air. *Energy Fuels* **2011**, *25*, 5528−5537.
(47) Marquez-Alvarez, C.; Žilkova, N.; Perez-Pariente, J.; Čejka, J. Synthesis, characterization and catalytic applications of organized mesoporous aluminas. *Catal. Rev.:Sci. Eng.* **2008**, *50*, 222−286.
(48) Stendardo, S.; Foscolo, P. U. Carbon dioxide capture with dolomite: a model for gas−solid reaction within the grains of a particulate sorbent. *Chem. Eng. Sci.* **2009**, *64*, 2343−2352.
(49) Harlick, P. J.; Sayari, A. Applications of pore-expanded mesoporous silica. 5. Triamine grafted material with exceptional CO_2 dynamic and equilibrium adsorption performance. *Ind. Eng. Chem. Res.* **2007**, *46*, 446−458.
(50) Potter, M. E.; Cho, K. M.; Lee, J. J.; Jones, C. W. Role of Alumina Basicity in CO_2 Uptake in 3-Aminopropylsilyl-Grafted Alumina Adsorbents. *ChemSusChem* **2017**, *10*, 2192−2201.
(51) Sircar, S.; Hufton, J. Why does the linear driving force model for adsorption kinetics work? *Adsorption* **2000**, *6*, 137−147.
(52) Glueckauf, E.; Coates, J. I. Theory of chromatography. Part IV. The influence of incomplete equilibrium on the front boundary of chromatograms and on the effectiveness of separation. *J. Chem. Soc.* **1947**, 1315−1321.

https://doi.org/10.1021/acs.iecr.4c04099
Ind. Eng. Chem. Res. 2025, 64, 2339−2353